ARTICLE IN PRESS

Developmental Biology ∎ (∎∎∎∎) ∎∎∎–∎∎∎

Contents lists available at ScienceDirect

Developmental Biology

journal homepage: www.elsevier.com/locate/developmentalbiology

In vivo analysis of hyaloid vasculature morphogenesis in zebrafish: A role for the lens in maturation and maintenance of the hyaloid

Andrea Hartsock, Chanjae Lee, Victoria Arnold, Jeffrey M. Gross *

Department of Molecular Biosciences, Institute for Cellular and Molecular Biology, The University of Texas at Austin, Austin, TX 78712, United States

ARTICLE INFO

Article history:
Received 6 June 2014
Received in revised form
28 July 2014
Accepted 30 July 2014

Keywords:
Zebrafish
Eye development
Hyaloid vasculature
Lens

ABSTRACT

Two vascular networks nourish the embryonic eye as it develops – the hyaloid vasculature, located at the anterior of the eye between the retina and lens, and the choroidal vasculature, located at the posterior of the eye, surrounding the optic cup. Little is known about hyaloid development and morphogenesis, however. To begin to identify the morphogenetic underpinnings of hyaloid formation, we utilized *in vivo* time-lapse confocal imaging to characterize morphogenesis of the zebrafish hyaloid through 5 days post fertilization (dpf). Our data segregate hyaloid formation into three distinct morphogenetic stages: Stage I: arrival of hyaloid cells at the lens and formation of the hyaloid loop; Stage II: formation of a branched hyaloid network; Stage III: refinement of the hyaloid network. Utilizing fixed and dissected tissues, distinct Stage II and Stage III aspects of hyaloid formation were quantified over time. Combining *in vivo* imaging with microangiography, we demonstrate that the hyaloid system becomes fully enclosed by 5 dpf. To begin to identify the molecular and cellular mechanisms underlying hyaloid morphogenesis, we identified a recessive mutation in the *mab21l2* gene, and in a subset of *mab21l2* mutants the lens does not form. Utilizing these "lens-less" mutants, we determined whether the lens was required for hyaloid morphogenesis. Our data demonstrate that the lens is not required for Stage I of hyaloid formation; however, Stages II and III of hyaloid formation are disrupted in the absence of a lens, supporting a role for the lens in hyaloid maturation and maintenance. Taken together, this study provides a foundation on which the cellular, molecular and embryologic mechanisms underlying hyaloid morphogenesis can be elucidated.

Introduction

The eye is a highly metabolic organ that requires substantial oxygen and nutrients for normal development. Two vascular networks nourish the embryonic eye as it develops - the hyaloid vasculature, located at the anterior of the eye between the retina and lens, and the choroidal vasculature, located at the posterior of the eye, surrounding the optic cup (reviewed in Saint-Geniez and D'Amore (2004)). The hyaloid artery enters the eye through the choroid fissure in the ventral optic cup, passes into the vitreous, and contacts the posterior pole of the lens. Here, the hyaloid artery branches over the posterior hemisphere of the lens to form the hyaloid network (known as the *tunica vasculosa lentis*). More anteriorly, the pupillary membrane branches from the hyaloid and covers the anterior of the lens. The hyaloid network connects to the choroidal network at the annular vessel, located along the anterior aspect of the optic cup, thereby providing drainage from the hyaloid, which contains no veins. The hyaloid vasculature is thought to form *via* angiogenesis, although recent data from human eyes indicate that the hyaloid system in humans may develop through hemo-vasculogenesis from a pool of hemangioblast precursors (McLeod et al., 2012). In mammals, the hyaloid system regresses during late stages of eye development, concomitant with the formation of the retinal vasculature (reviewed in Saint-Geniez and D'Amore (2004)). Defects in hyaloid regression result in persistent fetal vasculature, a congenital disorder that affects vision and may result in glaucoma, retinal detachment, cataract and strabismus if left untreated (reviewed in Shastry (2009)).

Little is known about hyaloid morphogenesis in the human eye, or in any animal model systems used to study eye development. Avian fate mapping studies have demonstrated that neural crest and mesoderm-derived cells enter the vitreous cavity at the time of hyaloid formation; periocular vessels are mesoderm-derived, and pericytes associated with the vessels are neural crest-derived (Johnston et al., 1979; Le Lievre and Le Douarin, 1975). Fate mapping studies in mouse have also demonstrated that both neural crest and mesoderm-derived cells contribute to the hyaloid (Gage et al., 2005). While studies have been performed to characterize the hyaloid in humans (Balazs et al., 1980;

* Corresponding author.
E-mail address: jmgross@austin.utexas.edu (J.M. Gross).

http://dx.doi.org/10.1016/j.ydbio.2014.07.024
0012-1606/

Please cite this article as: Hartsock, A., et al., *In vivo* analysis of hyaloid vasculature morphogenesis in zebrafish: A role for the lens in maturation and maintenance of the hyaloid. Dev. Biol. (2014), http://dx.doi.org/10.1016/j.ydbio.2014.07.024

McLeod et al., 2012; Zhu et al., 2000), primates (Hamming et al., 1977), mouse (Balazs et al., 1980; Gage et al., 2005; Poche et al., 2009), hamster, rabbit, cow, cat (Balazs et al., 1980) and zebrafish (Alvarez et al., 2007; Kitambi et al., 2009), most of these studies utilized fixed samples and were therefore unable to identify any of the dynamic cellular behaviors that underlie hyaloid formation.

With an interest in the cellular dynamics underlying hyaloid morphogenesis we re-examined hyaloid formation in zebrafish. Utilizing transgenic embryos that express GFP or RFP in the vasculature under control of the *fli1a* (Lawson and Weinstein, 2002) and *kdrl* (Wang et al., 2010) promoters, respectively, we performed *in vivo* time-lapse imaging of hyaloid formation. In combination with fixed sample analyses and microangiography, we describe and quantify dynamic aspects of hyaloid morphogenesis that were heretofore unknown. Specifically, hyaloid formation can be segregated into three distinct morphogenetic stages: Stage I – arrival of hyaloid precursors and formation of the "hyaloid loop", Stage II – formation of a branched hyaloid network, and Stage III – refinement and maturation of the network.

Studies in mice have shown that hyaloid development is influenced by both lens- and retinal-derived ligands, and the prevailing model is that tight control of VEGF availability is critical for normal hyaloid development (Ash and Overbeek, 2000; Garcia et al., 2009; Gerhardt et al., 2003; Mitchell et al., 2006; Rutland et al., 2007; Saint-Geniez et al., 2009). Zebrafish lens ablation studies suggest that the lens is not required for recruitment of hyaloid precursor cells to the eye (Semina et al., 2006); however, these lens ablations were performed at 24 hpf, a time point after hyaloid precursor cells have already arrived at the lens (this study). Moreover, it is unknown whether the lens is required for later stages of hyaloid development. To address these questions, we cloned the affected locus in a recessive zebrafish mutant in which a subset of homozygous embryos lack a lens (*mab21l2*^{au10}) (Lee et al., 2012), and used these lens-less mutants to assay hyaloid formation. Our results support a model in which hyaloid precursor recruitment and Stage I of hyaloid development do not require a lens, while Stage II and Stage III hyaloid growth and maturation are lens-dependent.

Materials and methods

Fish maintenance

Zebrafish (*Danio rerio*) were maintained at 28.5 °C on a 14-h-light/10-h-dark cycle. Embryos were obtained from the natural spawning of wildtype or heterozygous carriers set up in pairwise crosses. Alleles utilized in this study were Tg(*fli1a*:GFP^{y1Tg}); (Lawson and Weinstein, 2002), Tg(*kdrl*:mCherry^{is5}) (Wang et al., 2010) and *mab21l2*^{au10} (Lee et al., 2012). Animals were treated in accordance with University of Texas at Austin Institutional Animal Care and Use Committee provisions.

Cloning of mab21l2^{au10} *and mRNA rescue*

au10 Heterozygous carriers (AB background) were outcrossed with wild-type TU fish. Heterozygous carriers of the *au10* mutation were identified and then incrossed to generate homozygous mutant embryos. 50 mutant zebrafish embryos from 4 parental pairs were collected, genomic DNA was isolated (DNeasy Blood & Tissue Kit, Qiagen), and 1ug was used for Illumina sequencing at the UT Genomic Sequencing and Analysis Facility. 150 million paired-end 100 bp sequences were generated on an Illumina HiSeq 2000 machine, for an average genome coverage of 19 ×. To identify putative mutations, sequencing reads were analyzed using the BSFseq mapping pipeline on MegaMapper (Obholzer et al., 2012). Candidate SNPs were confirmed by cDNA sequencing. Full-length wild-type and mutant *mab21l2* were cloned from reverse transcribed zebrafish mRNA and then subcloned into CS10R-GFP for mRNA synthesis. RNA was synthesized using mMESSAGE mMACHINE SP6 Transcription kit (Life Technologies). One-cell embryos from *au10* were injected with 100 pg of mRNA of *mab21l2*-GFP and scored for lens defects; a subset of these were genotyped to verify rescue.

Cryosectioning and confocal imaging

Embryos were prepared for cryosectioning as previously described (Uribe and Gross, 2007). 20 μm sections were generated and imaged using a Leica TCS SP5 II fixed stage microscope with a 40 × (NA 1.3) objective taking 1 μm optical slices. Images were processed using Fiji.

In vivo imaging

One hour prior to imaging, embryos were anesthetized in 0.0015 M tricaine in fish water. 16 hpf–3 dpf embryos were submerged in 0.0015 M tricaine in 1% Low-Melt Agarose (LMA; UltraClean Agarose LM; #15005) while 3 dpf and older embryos were submerged in 0.0015 M tricaine in 1.2% LMA. Embryos were mounted in a glass-bottom imaging dish just below the LMA surface for imaging on an upright microscope equipped with immersion objectives, and at the glass surface for imaging on an inverted microscope. After 5 min at room temperature, mounted embryos were completely submerged in fish water with tricaine (0.0015 M). Embryos were either imaged using a Leica TCS SP5 II (upright) microscope using a 25 × immersion objective (NA 1.8) or a Zeiss Pascal (inverted) microscope under a 20 × objective (NA 0.8). 50–100, 1 μm optical slices were acquired every 10–15 min (see movie legends for details). Each stack was compressed to a maximum projection, and projections compressed to AVI formatted time series using Leica LAS or Zeiss LSM software. AVI files were adjusted for optimal viewing (i.e. brightness and contrast) using Fiji. Still images from movies were extracted post-optimization using Fiji. All movies play at 6 frames/s.

Lens dissections and imaging

Embryos were anesthetized in tricaine, fixed in 4% PFA and stored at 4 °C for 1–10 days. For dissection, embryos were submerged in PBS. Using insect pins the majority of retina was removed leaving a minimal amount of distal retinal tissue for orientation purposes, and lenses were then transferred to a glass-bottom imaging dish. Lenses were imaged on a Zeiss Pascal microscope under a 40 × objective (NA 1.3). Depending on lens size, 30–100 1 μm optical slices were obtained and maximum projections created using Zeiss LSM software. Lenses were imaged from the outer most visible edge to mid-hemisphere as indicated by the posterior coalescence of vessels.

Quantification of hyaloid formation in fixed lenses

Zeiss LSM software was used to measure the chord length (c) defined as the longest distance from the posterior hyaloid coalescence to the anterior most edge of the hyaloid (Fig. S1). The number of optical slices to image the outer most edge of the hyaloid to the most posterior coalescence of vessels was determined to be the radius (r). Arc length (A) was calculated as $A=r\theta$, where $\theta=2\sin^{-1}(c/2r)$ (Fig. S1). Branch number was also counted from maximum projections images. A student t-test was used to evaluate statistical significance (Microsoft Excel). Data are representative of one half of the hyaloid, imaged from a transverse view (Fig. S1).

Please cite this article as: Hartsock, A., et al., *In vivo* analysis of hyaloid vasculature morphogenesis in zebrafish: A role for the lens in maturation and maintenance of the hyaloid. Dev. Biol. (2014), http://dx.doi.org/10.1016/j.ydbio.2014.07.024

Microangiography and post-injection imaging

GFP$^+$ embryos were pre-screened in *fli1a*:GFP or *mab21l2*^{au10}; *fli1a*:GFP backgrounds. One hour prior to desired injection time, embryos were anesthetized using 0.0015 M tricaine in fish water. Embryos were then submerged in 0.0015 M tricaine in 2% LMA in fish water at room temperature against stacked and glued coverslips. Using a quartz 1.00 mm diameter microinjection needle, embryos were injected with 4.5 nL of 2.5% concentration of Rhodamine–dextran (50 kD) in 0.5 M KCl. Embryos 2 and 3 dpf were injected in the heart, while embryos 4 and 5 dpf were injected in the posterior caudal vein (Schmitt et al., 2012). Embryos were then re-mounted in 0.0015 M tricaine in 1% LMA on a glass coverslip for an inverted confocal scope. After 5 min at room temperature to solidify LMA, embryos were submerged in 0.0015 M tricaine in fish water. Utilizing a Zeiss Pascal confocal microscope under a 20× objective (NA 0.8), 30–100 1 m optical slices were obtained and maximum projections generated using Zeiss LSM software. Maximum projections were utilized to create iso-surface renderings in Imaris.

Results

Overview of in vivo imaging experiments

To image the developing hyaloid we utilized *fli1a*:GFP (Lawson and Weinstein, 2002) and *kdrl*:mCherry (Wang et al., 2010) transgenic lines, both of which label the developing hyaloid vasculature (Fig. S2). However, when utilizing *kdrl*:mCherry transgenics, mCherry was not detected within the hyaloid until 22 hpf and therefore all images prior to 22 hpf necessarily utilized *fli1a*:GFP. 22–72 hpf Embryos were mounted on their sides and optical slices were taken through the lens along its anterior–posterior axis (Fig. 1A-sagittal imaging). 3–5 dpf Embryos were mounted either dorsal-down or ventral-down and optical slices were collected along the dorsal–ventral axis of the lens (Fig. 4A-transverse imaging).

Stage I: arrival of hyaloid cells at the eye and formation of the hyaloid loop

Stage I of hyaloid formation results in the recruitment of hyaloid precursor cells to the vitreous/lens and the formation of the primitive hyaloid at the posterior of the lens. At 18–20 hpf, *fli1a*:GFP$^+$ cells arrive at the ventral eye and migrate through the choroid fissure toward the ventral lens (Fig. 1B; Supplementary Movie 1); at 21 hpf, they appear as a tube with multiple filopodial extensions emanating from the tip of the tube. At 24 hpf, the primitive hyaloid bifurcates, with one sprout angled nasally (Fig. 2A – arrowhead; Supplementary Movie 2), and the second sprout angled temporally (Fig. 2A – arrows, Supplementary Movie 2). The nasal branch continues to grow dorsally around the lens, until it meets cells from the temporal branch, which also extend

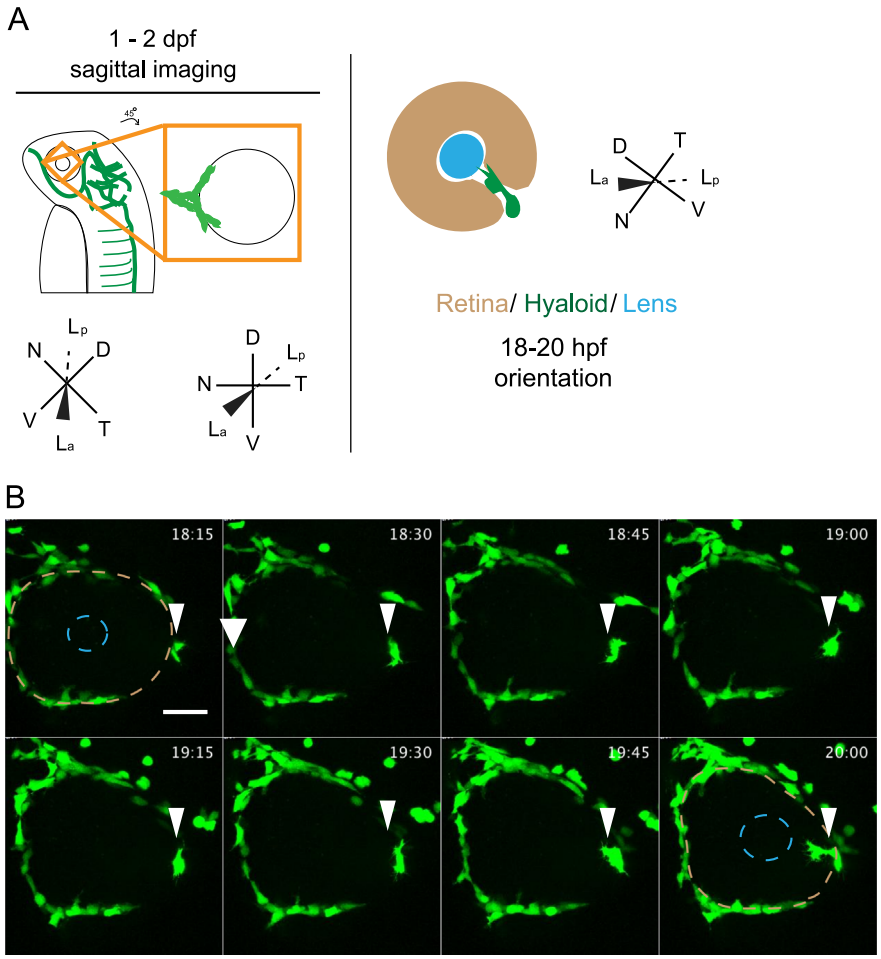

Fig. 1. Stage I: arrival of *fli1a*:GFP$^+$ cells at the ventral eye. (A) Schematic of 1–2 dpf imaging paradigm and maximum projection data. Drawings not to scale. (B) *fli1a*:GFP$^+$ cells (arrowheads) arrive at the ventral eye between 18 and 20 hpf. Precursor cells proceed towards the lens through the choroid fissure. Lens position indicated by dashed blue line, retina by dashed beige line. hh:mm. Scale bar = 50 μm D: Dorsal, V: Ventral, N: Nasal, T: Temporal, L_a: Lens anterior, L_p: Lens posterior.

Please cite this article as: Hartsock, A., et al., *In vivo* analysis of hyaloid vasculature morphogenesis in zebrafish: A role for the lens in maturation and maintenance of the hyaloid. Dev. Biol. (2014), http://dx.doi.org/10.1016/j.ydbio.2014.07.024

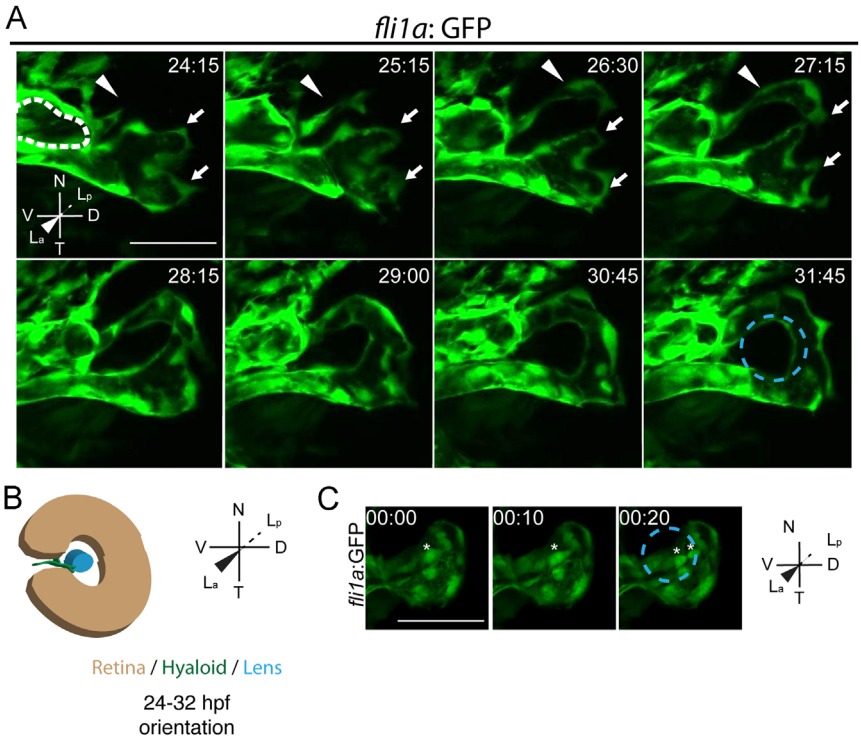

Fig. 2. Stage I: hyaloid loop formation. (A) Still maximum projection images from time-lapse movies highlighting formation of the hyaloid loop. Nasal (white arrow) and temporal (white arrowhead) oriented sprout morphogenesis to form the hyaloid loop. Dashed white line outlines cross section of vessel from which the hyaloid loop sprouts. (B) Schematic of maximum projection data. (C) Stills from time-lapse movie showing mitotic cells in the vessel stalk (asterisks) during formation of hyaloid loop. Lens position in B and C indicated by dashed blue line. hh:mm. All scale bars = 50 μm. D: Dorsal, V: Ventral, N: Nasal, T: Temporal, L_a: Lens anterior, L_p: Lens posterior.

dorsally (Fig. 2A; 24:15-28:15, Supplementary Movie 2). These two sprouts fuse to form a loop that cradles the posterior hemisphere of the lens ("the hyaloid loop"; Fig. 2A 27:15-31:45, Supplementary Movie 2). In optical cross section, the lumen of the vessel from which the hyaloid loop sprouts is evident (Fig. 2A – white dotted line). At later time points, this vessel will become the more distal hyaloid vessel within the choroid fissure (Fig. 3B – red asterisk).

Supplementary material related to this article can be found online at http://dx.doi.org/10.1016/j.ydbio.2014.07.024.

These imaging data support an angiogenic mechanism underlying Stage I of hyaloid vasculature formation. During angiogenesis, cellular extensions from a vessel are termed a vessel sprout; cells proximal to the originating vessel are termed 'stalk cells', and the most distal cell along the stalk is termed the 'tip cell'. These cell types are phenotypically distinct with tip cells possessing multiple filopodia, and stalk cells undergoing mitosis (reviewed in De Smet et al. (2009), Holderfield and Hughes (2008)). During Stage I hyaloid loop formation, the migration of tip and stalk cells toward the lens is evident, and mitosis in the stalk is also observed (Fig. 2C). Thus both cell movements and proliferation contribute to Stage I of hyaloid formation.

Stage II: formation of a branched hyaloid network

Stage II of hyaloid formation results in an expanded hyaloid that has spread from the posterior hemisphere of the lens towards the anterior hemisphere, and has formed an elaborately branched vessel network that encompasses the entire posterior of the lens. As with Stage I, Stage II growth and spreading of the hyaloid is the result of angiogenesis, as expansion of the hyaloid from the existing network is obvious in all time-lapse movies (Fig. 3). At ~32–33 hpf, the Stage I hyaloid loop has formed the nascent hyaloid basket located at the posterior of the lens (Fig. 3A,B; Supplementary Movie 3), and this is maintained until at least 5 dpf (Figs. 3–5).

Supplementary material related to this article can be found online at http://dx.doi.org/10.1016/j.ydbio.2014.07.024.

Hallmarks of Stage II are the substantial increases in vessel network density and complexity. These increases result from existing vessels breaking and forming new connections (Fig. 3C – asterisk; Supplementary Movie 4) and from angiogenic sprouting (Fig. 3C – arrows and arrowheads; Supplementary Movie 4). Sprouts are observed that find a vessel counterpart and form a new branch (Fig. 3C – arrows; Supplementary Movie 4), as well as those that do not and are resorbed into the originating vessel (Fig. 3C – arrowheads; Supplementary Movie 4). At ~69 hpf, the hyaloid network connects to the annular vessel (Fig. 3D – arrowhead; Supplementary Movie 5). Expansion of the hyaloid ultimately results in an intricately branched network spanning the posterior hemisphere of the lens, and connected to the annular vessel drainage system at the anterior.

Supplementary material related to this article can be found online at http://dx.doi.org/10.1016/j.ydbio.2014.07.024.

Stage III: refinement of the hyaloid network

Stage III of hyaloid formation results in a mature hyaloid that has decreased its overall number of branches. *In vivo* imaging demonstrates a progressive reduction in hyaloid network branches between 3 and 5 dpf (Fig. 4B). Moreover, time-lapse imaging at 72 hpf revealed that hyaloid vessels are connected by thin projections; over time, these connections break and the two vessels remain separated, thereby reducing the overall complexity of the network (Fig. 4C – asterisk; Supplementary Movie 6).

Supplementary material related to this article can be found online at http://dx.doi.org/10.1016/j.ydbio.2014.07.024.

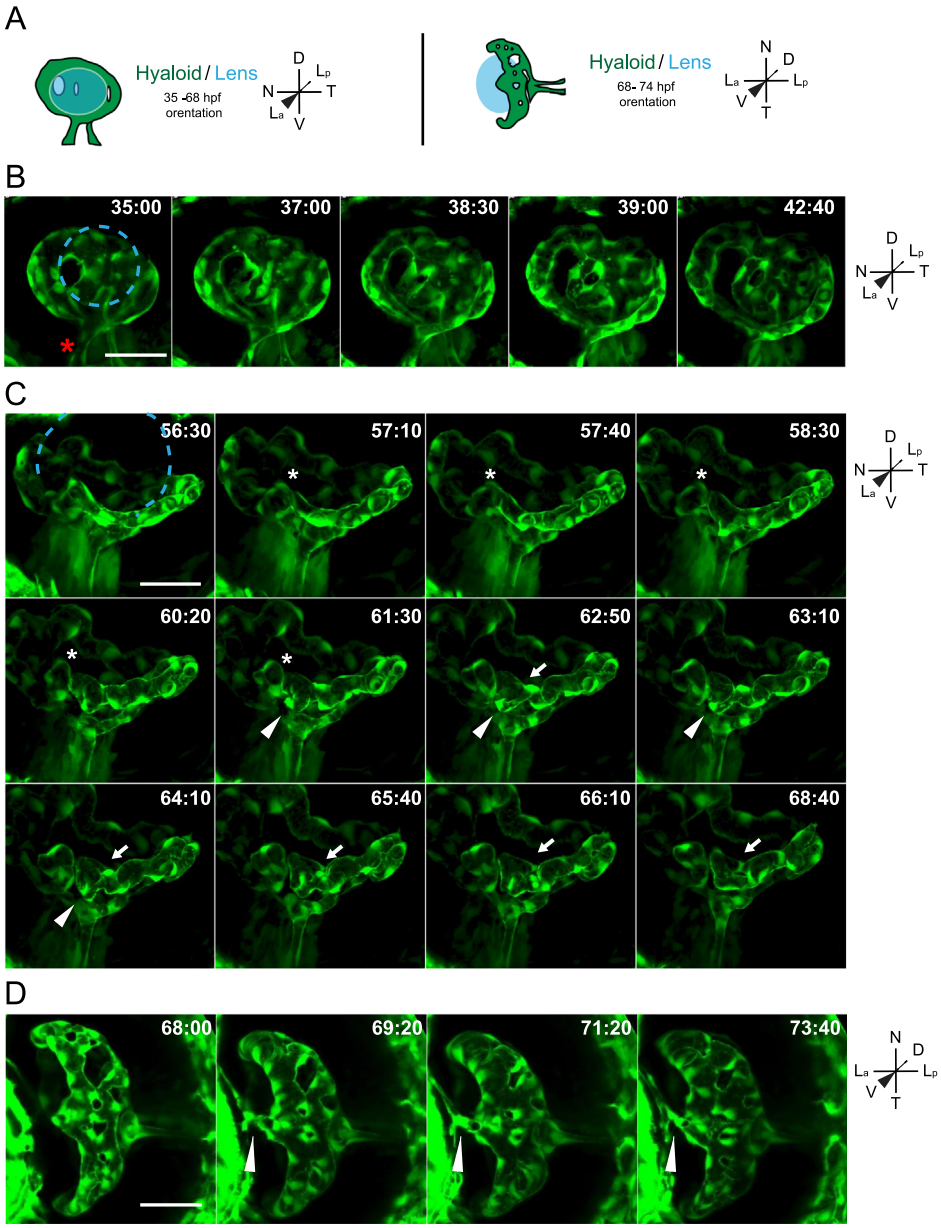

Fig. 3. Stage II: formation of a branched hyaloid network. All images are still maximum projections from time-lapse movies. (A) Schematic of imaging angles and maximum projection data. Drawings not to scale. (B) Increases in vessel network complexity within the posterior hyaloid. Asterisk marks the nasally oriented sprout of the hyaloid loop. (C) Angiogenesis within the hyaloid increases vessel network complexity. Asterisk marks site of break in vessel, arrowheads mark sprouting event that does not form a new connection, arrows mark sprouting event that generates a new loop within the vessel network. (D) Connection of the hyaloid to the annular ring (arrowhead). Lens position in B and C indicated by dashed blue line. hh:mm. Scale bars = 50 μm. D: Dorsal, V: Ventral, N: Nasal, T: Temporal, L_a: Lens anterior, L_p: Lens posterior.

Quantification of hyaloid growth

In vivo time-lapse imaging enables observations of dynamic cellular movements during hyaloid formation, but it is not practical to collect large sample sizes for quantification and statistical analyses of hyaloid formation. Therefore, we utilized lens dissections to quantify distinct aspects of hyaloid morphogenesis, specifically Stage II anterior progression and Stage III vessel refinement. 48 hpf was the earliest time point at which the lens could be removed from the optic cup with the hyaloid vasculature remaining attached. Stage II anterior progression was defined as the distance covered by the hyaloid basket along the posterior to anterior axis of the lens over time, and this was calculated by measuring the arc length of hyaloid vessels from maximum projection images of one half of the lens (Figs. 5A and S1; see "Materials and methods"). From 2 to 3 dpf, the hyaloid increases almost 400% in arc length, and this anterior growth continues from 3 to 5 dpf with statistically significant increases every 24 h (Fig. 5B). Stage III vessel refinement was defined as the reduction in branch points within the network over time, and was quantified by counting the number of identifiable hyaloid branches in maximum projection images. A statistically significant decrease in the number of branches occurs from 3 to 5 dpf (Fig. 5C).

The hyaloid system is fully enclosed at 5 dpf

Previous studies have attempted to determine when the zebrafish blood–retinal barrier (BRB) is formed and becomes functional by correlating tight junction localization and microangiography data (Hyoung Kim et al., 2011; Jeong et al., 2008; Xie et al., 2010). Results from these studies are confounding; the first reported a functional BRB that blocked a 4 kDa fluorescein dextran from

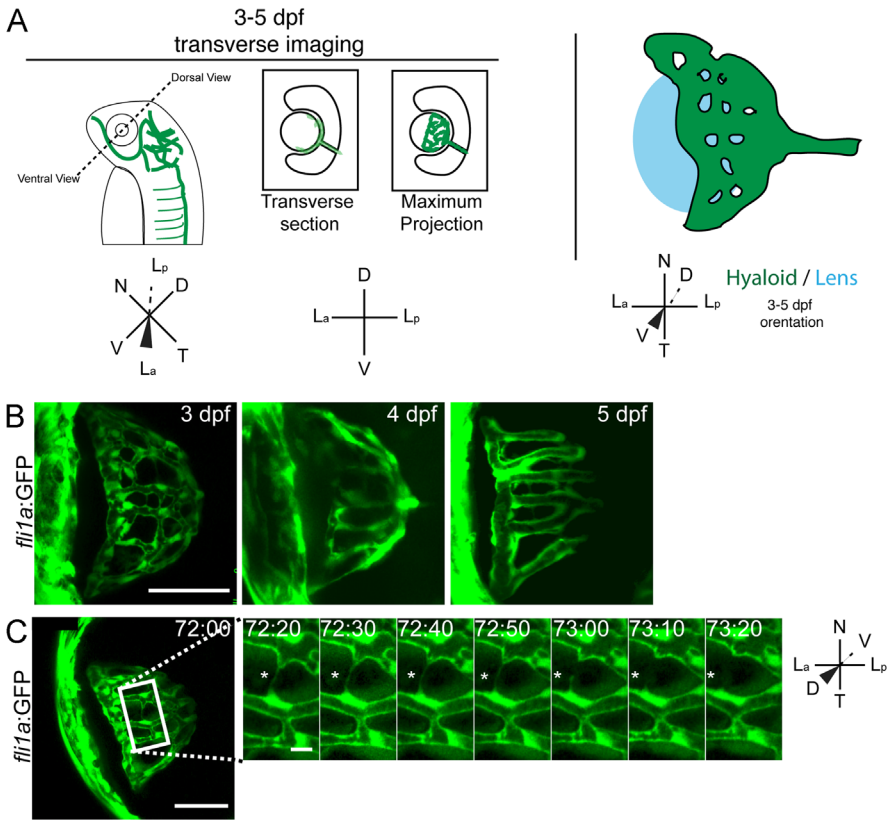

Fig. 4. Stage III: refinement of the hyaloid network. (A) Schematic of imaging angles and maximum projections data. Drawings not to scale. (B) Maximum projections of 3–5 dpf hyaloid in transverse imaging view demonstrating the continued reduction and refinement of the vessel network. (C) Still images from time-lapse movies demonstrating the further reduction in vessel complexity as fibers connecting adjacent vessels retract (asterisk). hh:mm. (A,B) Scale bar = 50μm; inset scale bar = 5 μm. D: Dorsal, V: Ventral, N: Nasal, T: Temporal, L_a: Lens anterior, L_p: Lens posterior.

leaking into the retina at 3 dpf (Xie et al., 2010); the second reported that a 10 kDa rhodamine dextran was not contained by the BRB at 3 dpf (Jeong et al., 2008); and the third reported that a 2000 kDa FITC–dextran was not contained at 7 dpf (Hyoung Kim et al., 2011). To distinguish between these studies we combined microangiography, using rhodamine dextran (50 kDa) injections and *in vivo* imaging in *fli1a*:GFP transgenic embryos through which we could immediately and unambiguously assess whether leakage into the retina or vitreous occurred. At 2 dpf, rhodamine was present throughout the vitreous, outside of *fli1a*:GFP$^+$ vessels, demonstrating that the hyaloid was not enclosed at this early time point (Fig. 6A). At 3 dpf, rhodamine was detected within hyaloid vessels (Fig. 6B – arrowheads), specifically those at the anterior limit of the hyaloid, but it was also detected outside of the hyaloid vessels more posteriorly (Fig. 6B – arrows). At 4 dpf, rhodamine was contained within dorsal hyaloid vessels (Fig. 6B – arrowheads), while ventral vessels remained leaky, with rhodamine detected within some vessels, but outside of others (Fig. 6B – arrows). By 5 dpf, rhodamine was completely contained within the hyaloid vessels (Fig. 6B). Thus, microangiography analyses demonstrate that hyaloid vessels steadily become lumenized, with the dorsal hyaloid vessels closing prior to ventral vessels, and both becoming fully enclosed by 5 dpf.

mab21l2^{au10} mutants do not form a lens

Hyaloid development can be influenced by lens-derived signals (Ash and Overbeek, 2000; Garcia et al., 2009; Rutland et al., 2007). However, a previous study utilizing a lens ablation paradigm did not identify a requirement for the lens in the recruitment of hyaloid precursor cells to the eye (Semina et al., 2006). In this study, lens ablations were performed at 24 hpf, and our *in vivo* imaging data demonstrate that recruitment of hyaloid precursor cells occurs at ~18–20 hpf, and the nascent hyaloid enters the eye at 21 hpf (Fig. 1B, Supplementary Movie 1). Thus, lens ablations were performed several hours after the nascent hyaloid had already entered the eye, making it unclear if, in fact, the lens is involved in the early stages of hyaloid development. To address this question, we utilized a recessive zebrafish mutant that lacked a lens, which had been identified from a forward genetic screen for mutations that affected eye development (Lee et al., 2012). The mutant, *au^{10}*, is variably penetrant with ~6.66 ± 1.2% of total embryos (~30% of mutants) possessing no obvious lens at 24 hpf (Fig. 7A-severe), and 16.41 ± 1.4% of total embryos (~70% of mutants) possessing a lens that is substantially reduced in size (Fig. 7A-mild). Histological analysis of the severe class of *au^{10}* mutants at 1 and 4 dpf highlights the complete absence of the lens (Fig. 7B). In addition to lens defects, the shape of the eye in *au^{10}* appears to be more oblong than round, and some embryos present with mild colobomas (Fig. 7A and *data not shown*).

To identify the gene mutated in *au^{10}*, we utilized next-generation sequencing and SNP mapping (Obholzer et al., 2012), generating ~19× average genome-wide sequencing coverage. Using the "MegaMapper" analysis pipeline, a 3 Mb window was identified on chromosome 1 that was predicted to harbor the mutation. The only "high-priority" candidate mutation within this region was an A to T transversion at nucleotide 301 of the *mab21l2* coding sequence (Fig. 7C). This mutation generates a premature stop codon at amino acid 101 (K101STOP; Fig. 7D), truncating the protein by ~66%. Sequencing of genomic DNA and cDNA from *au^{10}* mutants verified that the mutation segregated with all phenotypically mutant embryos (Fig. 7C).

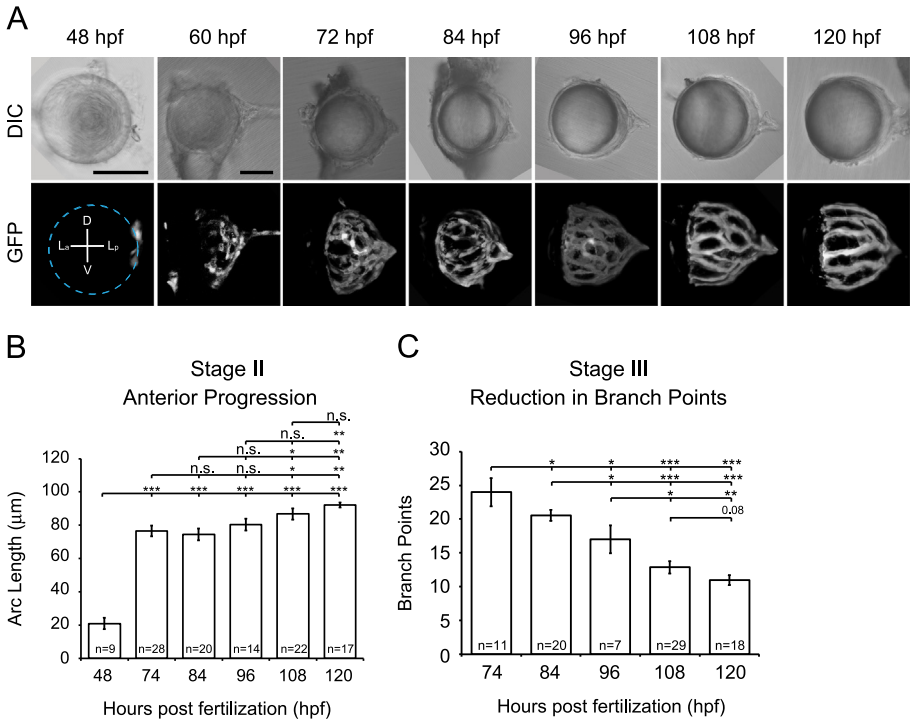

Fig. 5. Quantification of hyaloid growth. (A) DIC and GFP maximum projections images of dissected lenses from *fli1a*:GFP embryos at 12 h intervals from 2 to 5 dpf. Dashed line indicates location of the lens. Scale bars = 50 μm. D: Dorsal, V: Ventral, L_a: Lens anterior, L_p: Lens posterior (B) Quantification of anterior progression of the hyaloid over time. (C) Reduction in hyaloid vessel branching over time. $^{*}p \leq 0.01$, $^{**}p \leq 0.001$, $^{***}p \leq 1 \times 10^{-10}$. n = number of samples analyzed.

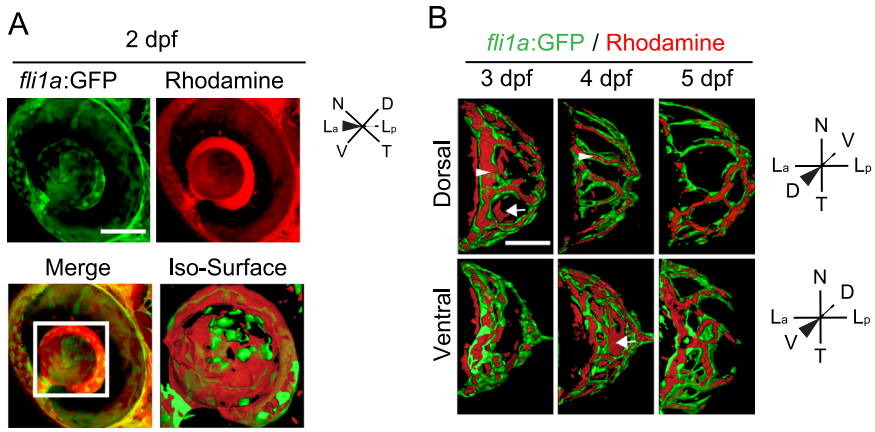

Fig. 6. Microangiography demonstrates that the hyaloid vessel is fully enclosed by 5 dpf. (A) Maximum projection images of the eye of a *fli1a*:GFP (green) embryo injected with 50 kDa rhodamine dextran (red). Merged image highlights that rhodamine is detected throughout the vitreous. Iso-surface rendering of merged image. (B–D) Iso-surface renderings of maximum projections collected from the eyes of 3–5 dpf *fli1a*:GFP (green) embryos injected with 50 kDa rhodamine dextran (red) and imaged either dorsally or ventrally. Arrowhead highlights rhodamine containment in a *fli1a*:GFP vessel and arrows highlight rhodamine outside of vessels. hh:mm. Scale bars = 50 μm. D: Dorsal, V: Ventral, N: Nasal, T: Temporal, L_a: Lens anterior, L_p: Lens posterior.

Originally identified in *C. elegans* as required for formation of sensory rays in the male tail (Chow et al., 1995), mab-21-family genes have been studied in a variety of organisms. In vertebrates, two mab-21 genes exist: mab21l1 and mab21l2. Mab21l1 is expressed in the mouse lens, and Mab21l1 knockouts do not form a lens (Yamada et al., 2003). Mab21l2 expression has been observed in the optic vesicle of mice (Wong et al., 1999), *Xenopus* (Baldessari et al., 2004) and zebrafish (Wong and Chow, 2002), and it is detected in human retinal extracts (Margolis et al., 1996). In zebrafish, *mab21l1* and *mab21l2* are both expressed in the developing optic cup at 11 hpf, with *mab21l1* becoming enriched in the retina at 24 hpf, and *mab21l2* expressed in the lens and dorsal and nasal aspects of the retina (Cederlund et al., 2011). These published data are consistent with the hypothesis that au^{10} possesses a mutation in *mab21l2*, and to validate this, mRNA rescue was performed. At 4 dpf, lens formation was normal in all embryos derived from au^{10} incrosses injected with *mab21l2-GFP* (n = 51; Fig. 7F). A subset of these were genotyped, and lens development was rescued in *mab21l2* mutants (n = 6; Fig. 7E), supporting that au^{10} is a mutation in *mab21l2* (hereafter referred to as $mab21l2^{au10}$).

Little is known about the cellular functions of mab21l2; a myc-tagged version of mouse Mab21l2 is localized to the nucleus when expressed in NIH3T3 cells (Mariani et al., 1999), and our GFP-tagged mab21l2 was also detected in the nucleus (*data not shown*). In a heterologous cell culture expression system, *Xenopus* Gal4-tagged Mab21l2 acts as a transcriptional repressor (Baldessari et al., 2004). The position of the nonsense mutation in $mab21l2^{au10}$

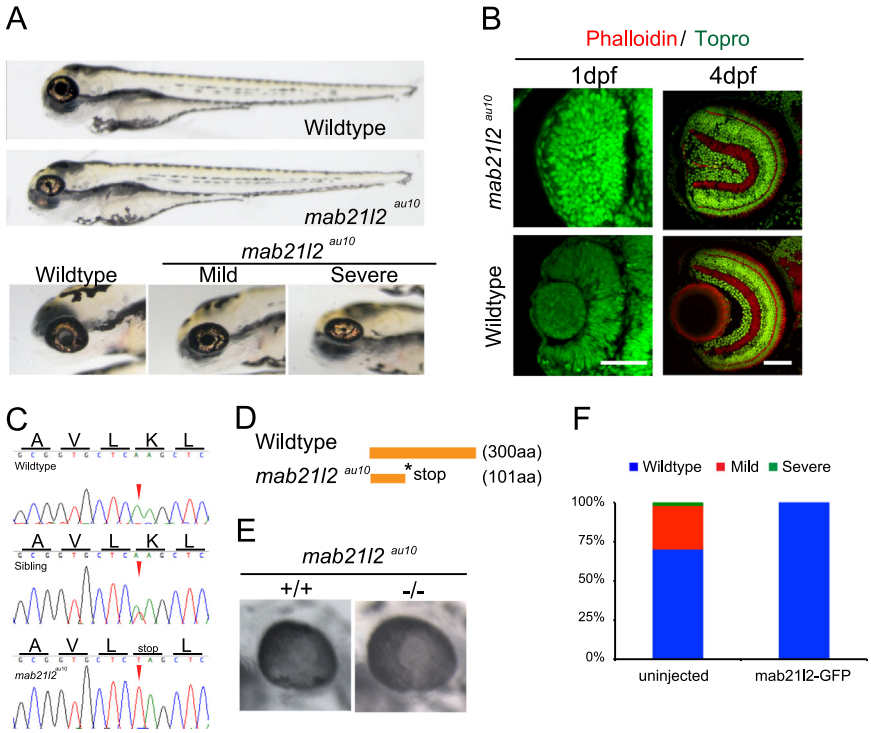

Fig. 7. *mab21l2*^{au10} mutants possess defects in lens formation. (A) Images of phenotypically wild-type sibling and *mab21l2*^{au10} mutants at 4 dpf. High-magnification views of the eyes of mild and severe *mab21l2* ^{au10} mutants. (B) Transverse cryossections of wild-type and severe *mab21l2*^{au10} mutants at 1 and 4 dpf highlighting the lack of a lens in severe *mab21l2*^{au10} mutants. Scale bars = 50 μm. (C) Genomic sequences from wild-type, heterozygous and *mab21l2*^{au10} mutants. *mab21l2*^{au10} mutants possess an A→T transversion at position 301, resulting in a premature stop codon at amino acid 101. (D) Schematic of protein length of wild-type and *mab21l2*^{au10} mutant. (E) High magnification view of eye in sibling (wild-type) and *mab21l2*^{au10} mutant embryo injected with *mab21l2-GFP* (rescue). (F) Quantification of lens phenotype after *mab21l2-GFP* injection.

mutants, truncating the mab21l2 protein by roughly two-thirds, suggests that the *au*^{10} allele may be a null. However, structure–function relationships for the mab2l12 protein are unknown, and no obvious conserved structural motifs are predicted from its sequence; therefore, the variable penetrance and expressivity of the phenotype in *mab21l2*^{au10} mutants could also possibly indicate that some function of the protein remains, and the *au*^{10} allele is a hypomorph.

The lens is required for Stages II and III of hyaloid formation

As discussed above, hyaloid development can be influenced by lens-derived signals, but it is unclear whether they lens is required for the recruitment of hyaloid precursor cells to the eye, or how the lens facilitates hyaloid maturation. With this in mind, we wanted to utilize *mab21l2*^{au10} mutants that lacked a lens as a tool through which we could address these outstanding questions. *mab21l2*^{au10}; *fli1a*:GFP embryos were generated, and we performed *in vivo* imaging of hyaloid formation, as above. Hyaloid arrival is delayed by ~2 h in *mab21l2*^{au10} mutants (Fig. 8A; Supplementary Movie 7), although by ~26 hpf, the hyaloid of *mab21l2* mutants was indistinguishable from that of wild-type embryos. Stage I hyaloid loop formation was normal, indicating that while lack of a lens may slightly delay the arrival of hyaloid precursor cells, the lens is not required for Stage I to progress (Supplementary Movie 8 and Fig. 8B up to 29:00, compare to Fig. 2A). *In vivo* imaging of Stages I–II of hyaloid formation in *mab21l2*^{au10} mutants revealed hyaloid cells that were highly active, possessing multiple filopodial extensions in all directions, but these cells did not assemble into obvious vessels (Fig. 8B,C; Supplementary Movies 7–9). In addition, the network appears collapsed and is skewed in the temporal direction (Fig. 8B; Supplementary Movie 8, compare to Fig. 2A). Interestingly, this phenotype was observed in both *mab21l2*^{au10} mutants that lacked a lens, as well as *mab21l2*^{au10} mutants with smaller lenses (Fig. S3A), suggesting that collapse of the hyaloid was not solely due to the lack of a lens (i.e. not the lack of a physical substrate). At 3 dpf, the *mab21l2*^{au10} mutant hyaloid extended to the distal retina and formed connections to the annular ring (Fig. 8D – arrowhead; Supplementary Movies 10 and 11), similar to wild-type embryos, but the hyaloid network retained its collapsed appearance (Fig. 8D – arrowheads; Supplementary Movies 10 and 11, compare to Figs. 1B and 2A). Importantly, examination of intersegmental vessel formation revealed no defects in the severe class of *mab21l2*^{au10} mutants (Fig. S3B), suggesting that the *mab21l2*^{au10} mutation itself does not result in general vascular defects. Finally, microangiography analyses of *mab21l2*^{au10} mutants demonstrated that while there is a lumenized and enclosed vessel leading into the hyaloid, the hyaloid vasculature in the distal retina is not enclosed (Fig. 8E).

Supplementary material related to this article can be found online at http://dx.doi.org/10.1016/j.ydbio.2014.07.024.

Discussion

The goal of this study was to characterize the highly dynamic morphogenesis of the hyaloid vasculature of the vertebrate eye, and to use these data to begin to dissect the molecular and cellular underpinnings of hyaloid development. Capitalizing on the strengths of the zebrafish system for *in vivo* imaging, we were able to observe hyaloid formation *in vivo* from ~1 to 5 dpf and identify key phases of this process, something that has not been performed previously in humans or any vertebrate model system. Indeed, data from previous studies in zebrafish, utilizing fixed and dissected lens samples, suggested that hyaloid formation initiates

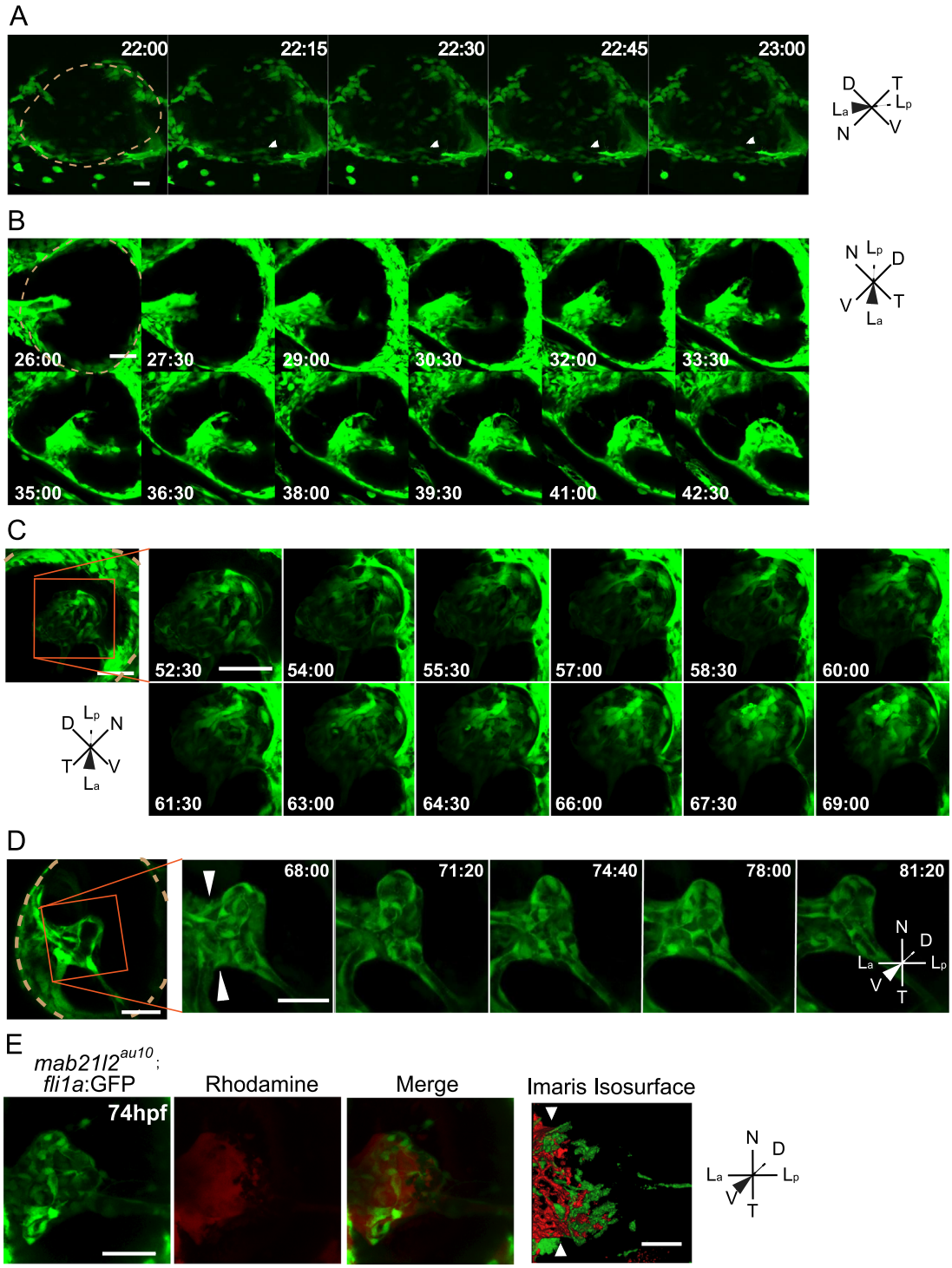

Fig. 8. The lens is required for Stages II and III hyaloid maturation and maintenance. All images are stills from time-lapse movies from severe *mab21l2*^{au10}; *fli1a*:GFP mutants. (A) Hyaloid precursor cell recruitment is delayed by ~2 h in *mab21l2*^{au10} mutants but recruitment is otherwise normal. (B) Hyaloid loop formation occurs in the absence of a lens. (C) Stage II formation of a branched hyaloid network is disrupted in *mab21l2*^{au10} mutants. Hyaloid cells appear disorganized and dynamic, having not coalesced into obvious vessels. (D) The hyaloid in *mab21l2*^{au10} mutants still makes contact anteriorly with the annular vessel. (E) Microangiography demonstrates that at 3d pf, the *mab21l2*^{au10} mutant hyaloid is not enclosed anteriorly, and rhodamine (red) fills the retina. hh:mm. Beige dashed line in A, B and D indicate outlines of the retina. All scale bars = 50 μm. D: Dorsal, V: Ventral, N: Nasal, T: Temporal, L_a: Lens anterior, L_p: Lens posterior.

at ~48–60 hpf (Alvarez et al., 2007). Our *in vivo* data, however, demonstrate that hyaloid development starts far earlier then this, with the first vascular cells detected in the eye between 18 and 20 hpf, and a morphologically obvious hyaloid present by 30 hpf. Moreover, from our *in vivo* data, in comparison to the Alvarez et al. (2007) study, the earliest phases of hyaloid development are far more complex than what can be identified from fixed samples (Alvarez et al., 2007). These data are consistent with studies by Kitambi et al. (2009) who detected *fli1a*:GFP cells around the lens at 24 hpf and a complex hyaloid at 48 hpf (Kitambi et al., 2009)

Our data segregate hyaloid formation into three distinct stages (summarized in Fig. 9). During Stage I, hyaloid precursor cells arrive at the lens and form the hyaloid loop at the posterior of the lens (Fig. 9A). In Stage II, the hyaloid system substantially

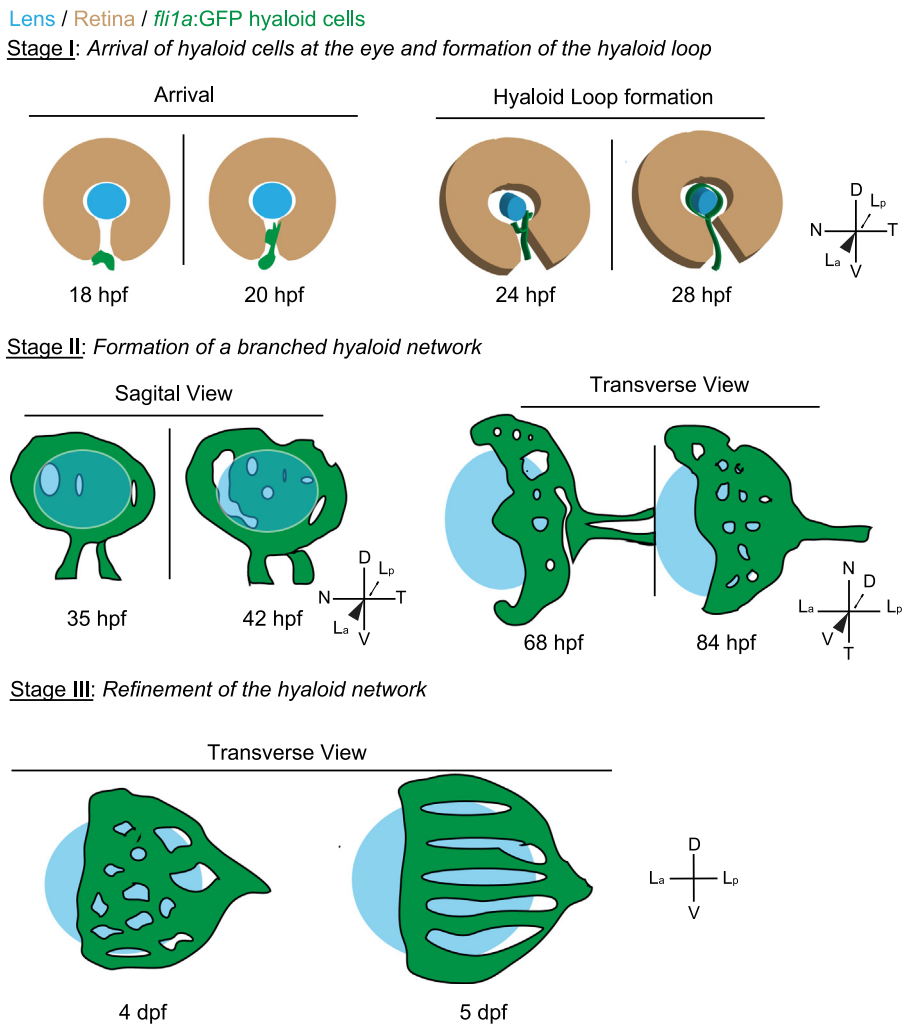

Fig. 9. Schematic depiction of hyaloid morphogenesis in zebrafish. See text for details of each stage. Drawings are not to scale.

elaborates into a branched hyaloid network (Fig. 9B). Throughout Stage III, the hyaloid network is refined, with an overall decrease in number of branches and the system becomes fully enclosed (Fig. 9C). In addition, utilizing fixed samples, we were able to demonstrate quantifiable landmarks that coincide with Stage II (anterior progression) and Stage III (branch point reduction). Finally, utilizing a recessive *mab21l2* mutant that does not form a lens, we were able to determine that the lens is not required for Stage I of hyaloid formation, but is required for Stages II and III of hyaloid maturation.

The mechanisms facilitating hyaloid formation have not been well studied. Highlighting this point, a recent study in zebrafish demonstrated that choroid fissure closure can be affected by defects in the developing hyaloid (Weiss et al., 2012). In this study, the hyaloid was severely dilated in *lmo2* mutants and this physically impeded closure of the choroid fissure, resulting in colobomas. Thus, not only is a functional hyaloid system required for growth of the eye, defects in hyaloid formation can contribute to other ocular malformations.

Angiogenic sprouting has been studied extensively in a variety of contexts including zebrafish intersegmental vessels and the mouse retina (reviewed in Eilken and Adams (2010)). While prevailing models suggest that hyaloid growth occurs through angiogenesis (*e.g.* (Saint-Geniez and D'Amore, 2004), recent data in the human eye suggest that hemo-vasculogenesis may build the hyaloid (McLeod et al., 2012). Our *in vivo* imaging data support an angiogenic mechanism for hyaloid development in zebrafish, and to our knowledge, these data are the first to demonstrate hyaloid angiogenesis *in vivo* in any vertebrate system. During angiogenesis, multi-cellular extensions emanate from existing vessels, and these extensions are polarized along their proximal–distal axes, with the proximal region comprised of stalk cells and the distal region containing a tip cell (Adams and Alitalo, 2007; Geudens and Gerhardt, 2011). The tip cells possesses numerous filopodial extensions that guide growth and branching of the vessels as they presumably encounter pro-and anti-angiogenic factors (reviewed in (Lamalice et al., 2007). From *in vivo* imaging of hyaloid formation, Stages I and II showed a tip cell sprouting mechanism to form the hyaloid loop and to increase the complexity of the vessel network, and this is similar to that observed in zebrafish intersegmental vessels (Lawson and Weinstein, 2002), and angiogenesis in the mouse retina (Ausprunk and Folkman, 1977; Fruttiger, 2007). Recently it was shown that during angiogenesis of the aorta and retina, tip cells are sometimes overtaken by stalk cells and this results in cell mixing during vessel formation (Arima et al., 2011). During Stage I of hyaloid morphogenesis, we did not detect any stalk cells overtaking tip cells, however we cannot rule out the possibility that stalk cells overtake tip cells during Stage II and contribute to the anterior progression of the hyaloid. Lineage tracing studies will be able to resolve this issue and determine the fates of individual hyaloid cells within the vessel network, as well as the morphogenetic mechanisms underlying hyaloid expansion

Stage III of hyaloid formation involves a remodeling of the hyaloid vasculature network by vessel pruning, leading to a

reduction in overall vasculature complexity. This quantifiable reduction in vascular complexity could result from retraction of vessel contacts within branches or from apoptosis of hyaloid cells within the vessels. Results from *in vivo* imaging indicate that branches retract, and this is similar to what has been observed during vascular remodeling in the zebrafish (Chen et al., 2012) and mouse brain (Wang et al., 1992). Interestingly, vasculature remodeling in the zebrafish brain results from a lack of blood flow into the vessels that are being pruned (Chen et al., 2012). Additionally, observations of Nasal Ciliary Artery pruning in zebrafish demonstrate that a pruned vessel becomes unicellular and elongated as it regresses from the maintained vessel network (Kochhan et al., 2013), similar to our observations of vessel remodeling in the hyaloid (Fig. 4). Our *in vivo* imaging of *fli1a*:GFP embryos indicate the final stage of hyaloid development is comprised of a reduction in vasculature complexity due to reduction in cell-cell connections. Although microangiography analysis provides insight into lumenization of the hyaloid, additional studies utilizing a transgenic line in which blood cells are labeled would be required to determine if lack of blood flow precedes hyaloid remodeling.

To begin to dissect the tissues required for hyaloid formation, we cloned a recessive mutation in *mab21l2*, and ~30% of *mab21l2*^{au10} mutants lacked lenses. Morpholino-mediated knockdown of *mab21l2* in zebrafish resulted in a range of ocular defects that included microphthalmia and delays in retinal differentiation (Kennedy et al., 2004). Mab21l2 morphants also displayed substantially elevated levels of apoptosis in their retinas at 24 hpf, and regions of persistent death at the retinal periphery at 3 dpf. While a lens did form in *mab21l2* morphants, the lens epithelium was abnormal and possibly undergoing apoptosis. Hyaloid vessels in *mab21l2* morphants were also reported to be thicker and poorly patterned at 5 dpf (Alvarez et al., 2007). These phenotypes are different than those observed in *mab21l2*^{au10} mutants, and could reflect maternal compensation in the mutants, or compensation from *mab21l1*, whose expression overlaps that of *mab21l2* in many regions of the embryo, including the retina (Cederlund et al., 2011). Despite truncating the protein by roughly two-thirds, the *mab21l2*^{au10} mutation could also be hypomorphic, and the truncated protein retains some of its endogenous function. Mab21l2 is not predicted to possess any conserved protein domains, and beyond localization to the nucleus when ectopically expressed (Mariani et al., 1999); CL, *unpublished observations*), little is known about the molecular functions of the protein. From a gene regulatory network perspective, *mab21l2* expression is regulated by Pax6 (Wolf et al., 2009) and it is thought to act upstream of gene products involved in early aspects of lens formation (Cvekl and Duncan, 2007; Yamada et al., 2004). Future studies will be needed to determine whether mab21l2 acts as a transcription factor, whether it binds DNA directly or as part of a complex, and what targets it regulates during lens formation.

With respect to hyaloid formation and the influence of the lens, our data demonstrate that hyaloid precursor cells were recruited to the optic cup/vitreous in *mab21l2* mutants although they were slightly delayed in their arrival, supporting a model in which the lens is not required for hyaloid precursor cell recruitment, though it may contribute to the process. Late Stage I (hyaloid loop formation) and Stages II and III of hyaloid morphogenesis were disrupted in *mab21l2* mutants, indicating that the lens is required for sustained hyaloid growth and maturation. VEGF expression within the lens is known to influence hyaloid development (Ash and Overbeek, 2000; Garcia et al., 2009; Rutland et al., 2007), so it is possible that in the absence of a VEGF source, growth and maintenance of the hyaloid are perturbed in *mab21l2* mutants. Alternatively, the lens is enclosed by the lens capsule, an extracellular matrix (ECM)-rich basement membrane on which the developing hyaloid resides. Previous studies in mice and zebrafish have demonstrated that ECM components of the lens capsule such as laminin alpha 1 and collagen are required for hyaloid development (Fukai et al., 2002; Rutland et al., 2007; Saint-Geniez et al., 2009). While mouse knockouts for many ECM components are embryonic lethal prior to lens formation (Alpy et al., 2005; Edwards et al., 2010; Francis et al., 2002; George et al., 1997, 1993; Miner et al., 2004), many zebrafish ECM mutants survive to 5–7 dpf providing models through which the later roles of these ECM components can be studied (Amsterdam et al., 2004; Karlstrom et al., 1996; Koshida et al., 2005; Parsons et al., 2002; Trinh and Stainier, 2004). The zebrafish lens capsule contains laminin-111 (Hayes et al., 2012; Lee and Gross, 2007), fibronectin (Hayes et al., 2012) and multiple collagens (Fang et al., 2010; Xiao and Baier, 2007). Thus, it is likely that these components are required for the growth and maturation of the hyaloid by providing a substrate on which the hyaloid cells migrate, or a signal that shapes their morphogenesis. Indeed, preliminary analyses of zebrafish *fibronectin1b* mutants suggest that the hyaloid is malformed (AH, *unpublished observations*). It will be interesting to utilize other zebrafish ECM mutants to determine how hyaloid formation is affected in the absence of distinct ECM components.

In summary, this study establishes a framework for *in vivo* imaging of hyaloid vasculature development in the zebrafish eye, providing a vertebrate model through which the cellular, molecular and embryologic mechanisms underlying distinct phases of hyaloid formation can be elucidated. Furthermore, it provides quantifiable landmarks that can be used for identifying defects in hyaloid morphogenesis. Finally, the results support a role for the lens in the maturation and maintenance of the hyaloid, but not in the initial stages of hyaloid formation.

Acknowledgements

We are grateful to Tom Waits for technical assistance, members of the Gross lab for helpful comments and criticisms on this work, Nikolaus Obholzer for advice on using Megamapper and to Jeff Essner for providing *kdrl*:mCherry^{is5} transgenics and helpful advice. AH thanks Dave Raible, Andres Collazo and Jim Fadool for advice on live imaging experiments provided during the Zebrafish Genetics and Development course at the Marine Biological Laboratories in Woods Hole, MA. This work was funded by the National Institutes of Health/National Eye Institute Grants RO1-EY18005, EY18005-04S1 and R21-EY22770 to JMG, and the University of Texas at Austin Undergraduate Research Fellowship to VA. In vivo imaging was performed on a confocal microscope funded by the NIH S10-RR028951. Zebrafish were obtained from ZIRC, which is supported by the NIH-NCRR Grant P40 RR012546.

Appendix A. Supporting information

Supplementary data associated with this article can be found in the online version at http://dx.doi.org/10.1016/j.ydbio.2014.07.024.

References

Adams, R.H., Alitalo, K., 2007. Molecular regulation of angiogenesis and lymphangiogenesis. Nat. Rev. Mol. Cell Biol. 8, 464–478.

Alpy, F., Jivkov, I., Sorokin, L., Klein, A., Arnold, C., Huss, Y., Kedinger, M., Simon-Assmann, P., Lefebvre, O., 2005. Generation of a conditionally null allele of the laminin alpha1 gene. Genesis 43, 59–70.

Alvarez, Y., Cederlund, M.L., Cottell, D.C., Bill, B.R., Ekker, S.C., Torres-Vazquez, J., Weinstein, B.M., Hyde, D.R., Vihtelic, T.S., Kennedy, B.N., 2007. Genetic determinants of hyaloid and retinal vasculature in zebrafish. BMC Dev. Biol. 7, 114.

Amsterdam, A., Nissen, R.M., Sun, Z., Swindell, E.C., Farrington, S., Hopkins, N., 2004. Identification of 315 genes essential for early zebrafish development. Proc. Natl. Acad. Sci. USA 101, 12792–12797.

Arima, S., Nishiyama, K., Ko, T., Arima, Y., Hakozaki, Y., Sugihara, K., Koseki, H., Uchijima, Y., Kurihara, Y., Kurihara, H., 2011. Angiogenic morphogenesis driven by dynamic and heterogeneous collective endothelial cell movement. Development 138, 4763–4776.

Ash, J.D., Overbeek, P.A., 2000. Lens-specific VEGF-A expression induces angioblast migration and proliferation and stimulates angiogenic remodeling. Dev. Biol. 223, 383–398.

Ausprunk, D.H., Folkman, J., 1977. Migration and proliferation of endothelial cells in preformed and newly formed blood vessels during tumor angiogenesis. Microvasc. Res. 14, 53–65.

Balazs, E.A., Toth, L.Z., Ozanics, V., 1980. Cytological studies on the developing vitreous as related to the hyaloid vessel system. Albrecht Von Graefes Arch. Klin. Exp. Ophthalmol. 213, 71–85.

Baldessari, D., Badaloni, A., Longhi, R., Zappavigna, V., Consalez, G.G., 2004. MAB21L2, a vertebrate member of the male-abnormal 21 family, modulates BMP signaling and interacts with SMAD1. BMC Cell Biol. 5, 48.

Cederlund, M.L., Vendrell, V., Morrissey, M.E., Yin, J., Gaora, P.O., Smyth, V.A., Higgins, D.G., Kennedy, B.N., 2011. mab21l2 Transgenics reveal novel expression patterns of mab21l1 and mab21l2, and conserved promoter regulation without sequence conservation. Dev. Dyn. 240, 745–754.

Chen, Q., Jiang, L., Li, C., Hu, D., Bu, J.W., Cai, D., Du, J.L., 2012. Haemodynamics-driven developmental pruning of brain vasculature in zebrafish. PLoS Biol. 10, e1001374.

Chow, K.L., Hall, D.H., Emmons, S.W., 1995. The mab-21 gene of Caenorhabditis elegans encodes a novel protein required for choice of alternate cell fates. Development 121, 3615–3626.

Cvekl, A., Duncan, M.K., 2007. Genetic and epigenetic mechanisms of gene regulation during lens development. Prog. Retin. Eye Res. 26, 555–597.

De Smet, F., Segura, I., De Bock, K., Hohensinner, P.J., Carmeliet, P., 2009. Mechanisms of vessel branching: filopodia on endothelial tip cells lead the way. Arterioscler. Thromb. Vasc. Biol. 29, 639–649.

Edwards, M.M., Mammadova-Bach, E., Alpy, F., Klein, A., Hicks, W.L., Roux, M., Simon-Assmann, P., Smith, R.S., Orend, G., Wu, J., Peachey, N.S., Naggert, J.K., Lefebvre, O., Nishina, P.M., 2010. Mutations in Lama1 disrupt retinal vascular development and inner limiting membrane formation. J. Biol. Chem. 285, 7697–7711.

Eilken, H.M., Adams, R.H., 2010. Dynamics of endothelial cell behavior in sprouting angiogenesis. Curr. Opin. Cell Biol. 22, 617–625.

Fang, M., Adams, J.S., McMahan, B.L., Brown, R.J., Oxford, J.T., 2010. The expression patterns of minor fibrillar collagens during development in zebrafish. Gene Expr. Patterns 10, 315–322.

Francis, S.E., Goh, K.L., Hodivala-Dilke, K., Bader, B.L., Stark, M., Davidson, D., Hynes, R.O., 2002. Central roles of alpha5beta1 integrin and fibronectin in vascular development in mouse embryos and embryoid bodies. Arterioscler. Thromb. Vasc. Biol. 22, 927–933.

Fruttiger, M., 2007. Development of the retinal vasculature. Angiogenesis 10, 77–88.

Fukai, N., Eklund, L., Marneros, A.G., Oh, S.P., Keene, D.R., Tamarkin, L., Niemela, M., Ilves, M., Li, E., Pihlajaniemi, T., Olsen, B.R., 2002. Lack of collagen XVIII/endostatin results in eye abnormalities. EMBO J. 21, 1535–1544.

Gage, P.J., Rhoades, W., Prucka, S.K., Hjalt, T., 2005. Fate maps of neural crest and mesoderm in the mammalian eye. Investig. Ophthalmol. Vis. Sci. 46, 4200–4208.

Garcia, C.M., Shui, Y.B., Kamath, M., DeVillar, J., Johnson, R.S., Gerber, H.P., Ferrara, N., Robinson, M.L., Beebe, D.C., 2009. The function of VEGF-A in lens development: formation of the hyaloid capillary network and protection against transient nuclear cataracts. Exp. Eye Res. 88, 270–276.

George, E.L., Baldwin, H.S., Hynes, R.O., 1997. Fibronectins are essential for heart and blood vessel morphogenesis but are dispensable for initial specification of precursor cells. Blood 90, 3073–3081.

George, E.L., Georges-Labouesse, E.N., Patel-King, R.S., Rayburn, H., Hynes, R.O., 1993. Defects in mesoderm, neural tube and vascular development in mouse embryos lacking fibronectin. Development 119, 1079–1091.

Gerhardt, H., Golding, M., Fruttiger, M., Ruhrberg, C., Lundkvist, A., Abramsson, A., Jeltsch, M., Mitchell, C., Alitalo, K., Shima, D., Betsholtz, C., 2003. VEGF guides angiogenic sprouting utilizing endothelial tip cell filopodia. J. Cell Biol. 161, 1163–1177.

Geudens, I., Gerhardt, H., 2011. Coordinating cell behaviour during blood vessel formation. Development 138, 4569–4583.

Hamming, N.A., Apple, D.J., Gieser, D.K., Vygantas, C.M., 1977. Ultrastructure of the hyaloid vasculature in primates. Investig. Ophthalmol. Vis. Sci. 16, 408–415.

Hayes, J.M., Hartsock, A., Clark, B.S., Napier, H.R., Link, B.A., Gross, J.M., 2012. Integrin alpha5/fibronectin1 and focal adhesion kinase are required for lens fiber morphogenesis in zebrafish. Mol. Biol. Cell 23, 4725–4738.

Holderfield, M.T., Hughes, C.C., 2008. Crosstalk between vascular endothelial growth factor, notch, and transforming growth factor-beta in vascular morphogenesis. Circ. Res. 102, 637–652.

Hyoung Kim, J., Suk Yu, Y., Kim, K.W., Hun Kim, J., 2011. Investigation of barrier characteristics in the hyaloid-retinal vessel of zebrafish. J. Neurosci. Res. 89, 921–928.

Jeong, J.Y., Kwon, H.B., Ahn, J.C., Kang, D., Kwon, S.H., Park, J.A., Kim, K.W., 2008. Functional and developmental analysis of the blood–brain barrier in zebrafish. Brain Res. Bull. 75, 619–628.

Johnston, M.C., Noden, D.M., Hazelton, R.D., Coulombre, J.L., Coulombre, A.J., 1979. Origins of avian ocular and periocular tissues. Exp. Eye Res. 29, 27–43.

Karlstrom, R.O., Trowe, T., Klostermann, S., Baier, H., Brand, M., Crawford, A.D., Grunewald, B., Haffter, P., Hoffmann, H., Meyer, S.U., Muller, B.K., Richter, S., van Eeden, F., Nusslein-Volhard, C., Bonhoeffer, F., 1996. Zebrafish mutations affecting retinotectal axon pathfinding. Development 123, 427–438.

Kennedy, B.N., Stearns, G.W., Smyth, V.A., Ramamurthy, V., van Eeden, F., Ankoudinova, I., Raible, D., Hurley, J.B., Brockerhoff, S.E., 2004. Zebrafish rx3 and mab21l2 are required during eye morphogenesis. Dev. Biol. 270, 336–349.

Kitambi, S.S., McCulloch, K.J., Peterson, R.T., Malicki, J.J., 2009. Small molecule screen for compounds that affect vascular development in the zebrafish retina. Mech. Dev. 126, 464–477.

Kochhan, E., Lenard, A., Ellertsdottir, E., Herwig, L., Affolter, M., Belting, H.G., Siekmann, A.F., 2013. Blood flow changes coincide with cellular rearrangements during blood vessel pruning in zebrafish embryos. PLoS One 8, e75060.

Koshida, S., Kishimoto, Y., Ustumi, H., Shimizu, T., Furutani-Seiki, M., Kondoh, H., Takada, S., 2005. Integrinalpha5-dependent fibronectin accumulation for maintenance of somite boundaries in zebrafish embryos. Dev. Cell 8, 587–598.

Lamalice, L., Le Boeuf, F., Huot, J., 2007. Endothelial cell migration during angiogenesis. Circ. Res. 100, 782–794.

Lawson, N.D., Weinstein, B.M., 2002. In vivo imaging of embryonic vascular development using transgenic zebrafish. Dev. Biol. 248, 307–318.

Le Lievre, C.S., Le Douarin, N.M., 1975. Mesenchymal derivatives of the neural crest: analysis of chimaeric quail and chick embryos. J. Embryol. Exp. Morphol. 34, 125–154.

Lee, J., Cox, B.D., Daly, C.M., Lee, C., Nuckels, R.J., Tittle, R.K., Uribe, R.A., Gross, J.M., 2012. An ENU mutagenesis screen in zebrafish for visual system mutants identifies a novel splice-acceptor site mutation in patched2 that results in Colobomas. Investig. Ophthalmol. Vis. Sci. 53, 8214–8221.

Lee, J., Gross, J.M., 2007. Laminin beta1 and gamma1 containing laminins are essential for basement membrane integrity in the zebrafish eye. Investig. Ophthalmol. Vis. Sci. 48, 2483–2490.

Margolis, R.L., Stine, O.C., McInnis, M.G., Ranen, N.G., Rubinsztein, D.C., Leggo, J., Brando, L.V., Kidwai, A.S., Loev, S.J., Breschel, T.S., Callahan, C., Simpson, S.G., DePaulo, J.R., McMahon, F.J., Jain, S., Paykel, E.S., Walsh, C., DeLisi, L.E., Crow, T.J., Torrey, E.F., Ashworth, R.G., Macke, J.P., Nathans, J., Ross, C.A., 1996. cDNA cloning of a human homologue of the Caenorhabditis elegans cell fate-determining gene mab-21: expression, chromosomal localization and analysis of a highly polymorphic (CAG)n trinucleotide repeat. Hum. Mol. Genet. 5, 607–616.

Mariani, M., Baldessari, D., Franciscono, S., Viggiano, L., Rocchi, M., Zappavigna, V., Malgaretti, N., Consalez, G.G., 1999. Two murine and human homologs of mab-21, a cell fate determination gene involved in Caenorhabditis elegans neural development. Hum. Mol. Genet. 8, 2397–2406.

McLeod, D.S., Hasegawa, T., Baba, T., Grebe, R., Galtier d'Auriac, I., Merges, C., Edwards, M., Lutty, G.A., 2012. From blood islands to blood vessels: morphologic observations and expression of key molecules during hyaloid vascular system development. Investig. Ophthalmol. Vis. Sci. 53, 7912–7927.

Miner, J.H., Li, C., Mudd, J.L., Go, G., Sutherland, A.E., 2004. Compositional and structural requirements for laminin and basement membranes during mouse embryo implantation and gastrulation. Development 131, 2247–2256.

Mitchell, C.A., Rutland, C.S., Walker, M., Nasir, M., Foss, A.J., Stewart, C., Gerhardt, H., Konerding, M.A., Risau, W., Drexler, H.C., 2006. Unique vascular phenotypes following over-expression of individual VEGFA isoforms from the developing lens. Angiogenesis 9, 209–224.

Obholzer, N., Swinburne, I.A., Schwab, E., Nechiporuk, A.V., Nicolson, T., Megason, S. G., 2012. Rapid positional cloning of zebrafish mutations by linkage and homozygosity mapping using whole-genome sequencing. Development 139, 4280–4290.

Parsons, M.J., Pollard, S.M., Saude, L., Feldman, B., Coutinho, P., Hirst, E.M., Stemple, D.L., 2002. Zebrafish mutants identify an essential role for laminins in notochord formation. Development 129, 3137–3146.

Poche, R.A., Larina, I.V., Scott, M.L., Saik, J.E., West, J.L., Dickinson, M.E., 2009. The Flk1-myr:mCherry mouse as a useful reporter to characterize multiple aspects of ocular blood vessel development and disease. Dev. Dyn. 238, 2318–2326.

Rutland, C.S., Mitchell, C.A., Nasir, M., Konerding, M.A., Drexler, H.C., 2007. Microphthalmia, persistent hyperplastic hyaloid vasculature and lens anomalies following overexpression of VEGF-A188 from the alphaA-crystallin promoter. Mol. Vis. 13, 47–56.

Saint-Geniez, M., D'Amore, P.A., 2004. Development and pathology of the hyaloid, choroidal and retinal vasculature. Int. J. Dev. Biol. 48, 1045–1058.

Saint-Geniez, M., Kurihara, T., Sekiyama, E., Maldonado, A.E., D'Amore, P.A., 2009. An essential role for RPE-derived soluble VEGF in the maintenance of the choriocapillaris. Proc. Natl. Acad. Sci. USA 106, 18751–18756.

Schmitt, C.E., Holland, M.B., Jin, S.W., 2012. Visualizing vascular networks in zebrafish: an introduction to microangiography. Methods Mol. Biol. 843, 59–67.

Semina, E.V., Bosenko, D.V., Zinkevich, N.C., Soules, K.A., Hyde, D.R., Vihtelic, T.S., Willer, G.B., Gregg, R.G., Link, B.A., 2006. Mutations in laminin alpha 1 result in complex, lens-independent ocular phenotypes in zebrafish. Dev. Biol. 299, 63–77.

Shastry, B.S., 2009. Persistent hyperplastic primary vitreous: congenital malformation of the eye. Clin. Exp. Ophthalmol. 37, 884–890.

Trinh, L.A., Stainier, D.Y., 2004. Fibronectin regulates epithelial organization during myocardial migration in zebrafish. Dev. Cell 6, 371–382.

Uribe, R.A., Gross, J.M., 2007. Immunohistochemistry on cryosections from embryonic and adult zebrafish eyes. CSH Protoc. 2007 (pdb prot4779).

Wang, D.B., Blocher, N.C., Spence, M.E., Rovainen, C.M., Woolsey, T.A., 1992. Development and remodeling of cerebral blood vessels and their flow in

postnatal mice observed with in vivo videomicroscopy. J. Cereb. Blood Flow Metab. 12, 935–946.

Wang, Y., Kaiser, M.S., Larson, J.D., Nasevicius, A., Clark, K.J., Wadman, S.A., Roberg-Perez, S.E., Ekker, S.C., Hackett, P.B., McGrail, M., Essner, J.J., 2010. Moesin1 and Ve-cadherin are required in endothelial cells during in vivo tubulogenesis. Development 137, 3119–3128.

Weiss, O., Kaufman, R., Michaeli, N., Inbal, A., 2012. Abnormal vasculature interferes with optic fissure closure in lmo2 mutant zebrafish embryos. Dev. Biol. 369, 191–198.

Wolf, L.V., Yang, Y., Wang, J., Xie, Q., Braunger, B., Tamm, E.R., Zavadil, J., Cvekl, A., 2009. Identification of pax6-dependent gene regulatory networks in the mouse lens. PLoS One 4, e4159.

Wong, R.L., Chan, K.K., Chow, K.L., 1999. Developmental expression of Mab21l2 during mouse embryogenesis. Mech. Dev. 87, 185–188.

Wong, R.L., Chow, K.L., 2002. Depletion of Mab21l1 and Mab21l2 messages in mouse embryo arrests axial turning, and impairs notochord and neural tube differentiation. Teratology 65, 70–77.

Xiao, T., Baier, H., 2007. Lamina-specific axonal projections in the zebrafish tectum require the type IV collagen Dragnet. Nat. Neurosci. 10, 1529–1537.

Xie, J., Farage, E., Sugimoto, M., Anand-Apte, B., 2010. A novel transgenic zebrafish model for blood–brain and blood–retinal barrier development. BMC Dev. Biol. 10, 76.

Yamada, R., Mizutani-Koseki, Y., Hasegawa, T., Osumi, N., Koseki, H., Takahashi, N., 2003. Cell-autonomous involvement of Mab21l1 is essential for lens placode development. Development 130, 1759–1770.

Yamada, R., Mizutani-Koseki, Y., Koseki, H., Takahashi, N., 2004. Requirement for Mab21l2 during development of murine retina and ventral body wall. Dev. Biol. 274, 295–307.

Zhu, M., Madigan, M.C., van Driel, D., Maslim, J., Billson, F.A., Provis, J.M., Penfold, P. L., 2000. The human hyaloid system: cell death and vascular regression. Exp. Eye Res. 70, 767–776.

Please cite this article as: Hartsock, A., et al., *In vivo* analysis of hyaloid vasculature morphogenesis in zebrafish: A role for the lens in maturation and maintenance of the hyaloid. Dev. Biol. (2014), http://dx.doi.org/10.1016/j.ydbio.2014.07.024